AIP | Journal of Applied Physics

Resonant planar antenna as an inductive plasma source

Ph. Guittienne, S. Lecoultre, P. Fayet, J. Larrieu, A. A. Howling et al.

Citation: J. Appl. Phys. **111**, 083305 (2012); doi: 10.1063/1.4705978

View online: http://dx.doi.org/10.1063/1.4705978

View Table of Contents: http://jap.aip.org/resource/1/JAPIAU/v111/i8

Published by the American Institute of Physics.

Resonant planar antenna as an inductive plasma source

Ph. Guittienne,[1,a)] S. Lecoultre,[2,b)] P. Fayet,[3] J. Larrieu,[3] A. A. Howling,[2] and Ch. Hollenstein[2]

[1]*HELYSSEN Sàrl, Route de la Louche 31, 1092 Belmont-sur-Lausanne, Switzerland*
[2]*Centre de Recherches en Physique des Plasmas, EPFL, 1015 Lausanne, Switzerland*
[3]*Tetra Pak (Suisse) SA, D&E, Advanced Film and Barrier Solutions, CP 32, 1680 Romont, Switzerland*

(Received 7 September 2011; accepted 22 March 2012; published online 27 April 2012)

A resonant planar antenna as an inductive plasma source operating at 13.56 MHz inside a low pressure vacuum vessel is presented for potential plasma processing applications. Its principle consists in interconnecting elementary resonant meshes composed of inductive and capacitive elements. Due to its structure, the antenna shows a set of resonant modes associated with peaks of the real input impedance. Each of these modes is defined by its own current and voltage distribution oscillating at the frequency of the mode. A rectangular antenna of 0.55 m $\times$ 0.20 m has been built, and first results obtained with argon plasmas are presented. Plasma generation is shown to be efficient as densities up to $4 \cdot 10^{17}\,\mathrm{m}^{-3}$ at 2000 W have been measured by microwave interferometry at a distance of 4 cm from the source plane. It is also demonstrated that the plasma couples inductively with the resonating currents flowing in the antenna above a threshold power of about 60 W. A non-uniformity of less than $\pm 5\%$ is obtained at 1000 W at a few centimeters above the antenna over 75% of its surface. [http://dx.doi.org/10.1063/1.4705978]

I. INTRODUCTION

Large area plasma processing[1–3] (typically over 1 m^2) is particularly interesting for developing new products in domains such as large area flat panel displays, packaging, and thin film solar cells. Even for wafer based processes, large area processing will allow much larger amounts of pieces to be treated at the same time, thus increasing the production throughput. The process rate relies essentially on the ability of the plasma sources to generate high electron densities and high dissociation rates of the precursors.

In one approach, parallel plate capacitively coupled reactors were successfully developed for large area processes. A major drawback is the low plasma density of capacitively coupled discharges (typically $10^{15} - 10^{16}$ electrons/m^3).[4] The deposition rates are limited because the high bombardment energy associated with high voltage sheaths can damage the growing film. Limits in the up-scaling of these reactors are due to their very low impedance, which implies high currents and voltages and therefore possible arcing and parasitic discharges, for example, in the power feeding line.

In another approach, the development of inductively coupled plasma (ICP) sources in the last 20 years has been motivated by the requirement of high densities (in the order of $10^{18}\mathrm{m}^{-3}$) and dissociation rates.[5] The first inductive plasmas for relatively large area processes were generated by spiral inductive couplers. Electrical problems arise, however, for diameters above 20–30 cm due to the high RF voltages required at the feeding of the inductor to sustain the high plasma density. Furthermore, as the inductance increases with size, the tuning capacitor to maintain the RF resonance frequency has to be decreased to values comparable with stray capacitances. The "ladder antenna" has been developed as an alternative configuration to increase the processed area. Indeed, a structure with inductive legs in parallel can reduce the reactive impedance.[6] Uniform plasma glow is obtained by choosing feeding, and earth points for which all currents paths have equal lengths and impedances. Drawbacks of this antenna design for plasma processing consists in the fact that its input impedance is principally reactive, which implies limited currents in the segments and therefore limited plasma density. The matching circuit of a reactive system very often limits the RF power, as it implies large dissipation.

In this paper, Sec. II presents the principles of a resonant planar antenna. Section III presents the experimental design of a RF plasma source operating at 13.56 MHz inside a low pressure vacuum vessel, suitable for both large area processing and high electron density. It can be designed in principle up to very large sizes by adding in series inductive copper legs linked together by capacitors. The resulting structure consists of a resonant circuit with modes of excitation characterized by high Q-factors. A semi-industrial plasma source of 0.55 m $\times$ 0.20 m has been built and tested up to 2 kW. The results in Sec. IV demonstrate that it produces a dense and uniform argon plasma by inductive coupling with the resonating currents.

II. PRINCIPLES OF THE HELYSSEN PLANAR ANTENNA

The present section describes briefly the principles of the HELYSSEN planar antenna.[7,8] Its structure and operating principles are similar to the closed cylindrical birdcage antenna previously described,[9,10] but it has been unwrapped to form an open and planar structure as shown in Figure 1. The planar antenna is suited for large area surface treatment,

[a)]Electronic mail: guittienne@helyssen.com.
[b)]Present address: Glas Tröesch AG, R&D coatings, Industriestrasse 29, CH-4922 Buetzberg, Switzerland.

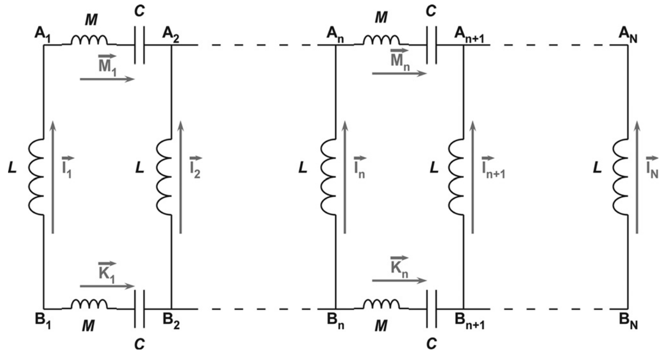

FIG. 1. Electrical circuit of the planar RF antenna.

whereas the cylindrical version is adapted to plasma processes requiring a volume plasma source. In both cases, the N parallel legs of the antenna are made of copper tubes which can be taken to act essentially as inductive elements of inductance L. High Q capacitors of capacitance C link the legs together and present also a small inductance M formed by the metallic leads. A complete analysis with detailed calculations of the RF circuit of the HELYSSEN antenna will follow in an upcoming publication.

Considering the ideal non-dissipative case, the impedance of the legs, and the impedance of segments containing a capacitor are purely imaginary.

Solving the Kirchhoff equations over the antenna with the open boundary conditions of the planar structure gives $N-1$ resonant modes m that arise from the parallel assembly of L and C components. Each of these modes is characterized by a resonance frequency ω_m and by specific current distributions in each segment I_n, M_n, and K_n and voltage distributions at the nodes A_n and B_n. The resonance frequencies are given by[9]

$$\omega_m = \frac{1}{\sqrt{C\left(M + 2L\sin^2\left(\frac{m\pi}{2N}\right)\right)}}, \quad \text{with } m \in [1, N-1]. \tag{1}$$

Assuming that the antenna is excited at one of its resonance frequencies by an excitation potential $V_{\text{in}} = V_0 \cdot \cos(\omega t)$ at the feeding node A_{N_f} and grounded at node A_{N_g}, the expressions for the leg currents I_n and capacitor currents M_n and K_n simplify to

$$\begin{cases} I_n = \dfrac{2V_0}{DL\omega_m} \cdot \cos(k_m(2n-1))\sin(\omega t) \\ M_n = -K_n = \dfrac{V_0}{DL\omega_m} \cdot \left(\dfrac{\sin(2k_m n)}{\sin(k_m)}\right)\sin(\omega t), \end{cases} \tag{2}$$

with $k_m = \frac{m\pi}{2N}$.

The voltages A_n and B_n at the nodes can be expressed as follows:

$$\begin{cases} A_n = \dfrac{V_0}{D}(\cos(k_m(2n-1)) - \cos(k_m(2N_g-1)))\cos(\omega t) \\ B_n = -\dfrac{V_0}{D}(\cos(k_m(2n-1)) + \cos(k_m(2N_g-1)))\cos(\omega t), \end{cases} \tag{3}$$

where

$$D = \cos(k_m(2N_f - 1)) - \cos(k_m(2N_g - 1)). \tag{4}$$

Note that these equations all have sinusoidal forms and oscillate temporally in phase. The spatial wavelength is inversely proportional to the mode number m. For instance, three normalized distributions are shown in Figure 2 corresponding to the modes $m=1$, $m=2$, and $m=6$ for a 23-leg antenna. Note that the current intensities in the legs for the $m=1$ mode constitute a half wavelength over the antenna length, while three wavelengths occur for the mode $m=6$.

III. THE EXPERIMENTAL HELYSSEN PLANAR ANTENNA

An experimental antenna has been built and tested with argon as working gas up to 2 kW for potential plasma processing applications. As shown in Figure 3(a), the antenna consists of 23 copper tubes $L_b = 0.2$ m assembled in parallel over a total length $L_a = 0.55$ m. The antenna is embedded in a silicone elastomer dielectric with a protective glass cover and a grounded metal baseplate as shown in Figure 3(b); this assembly constitutes the plasma source module which is entirely placed within a vacuum vessel. In this way, the antenna plasma source module is directly exposed to the low pressure plasma and does not need a separate dielectric window thick enough to withstand atmospheric pressure over the large area of the antenna. An insulating substrate could be placed directly on the antenna, with a gas showerhead placed opposite for uniform processing with reactive gases. Alternatively, any substrate could be positioned as an upper boundary of the plasma as shown in Fig. 3(b), in which case a gas showerhead could be incorporated into the antenna assembly.

Note that the antenna can be adapted to larger area processes, even up to meters of length, since the distributions of currents and voltages do not depend on these geometrical parameters. This property is one of the key advantages of this type of RF plasma source in comparison with other existing large area sources. In this particular configuration, there

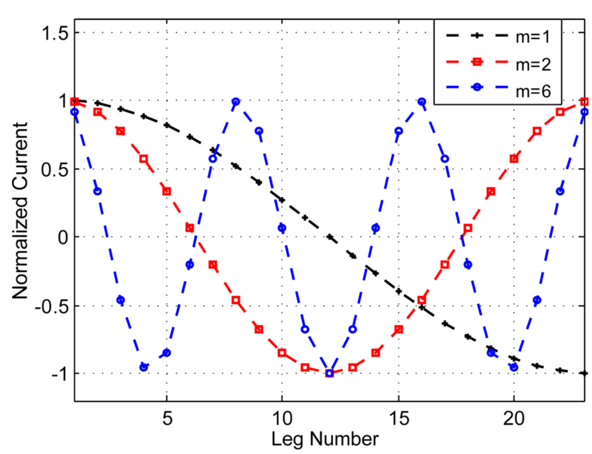

FIG. 2. Current distributions in the conductive legs for different modes of a 23-leg RF antenna. The symbols indicate the currents in each leg; the lines show the mode structure.

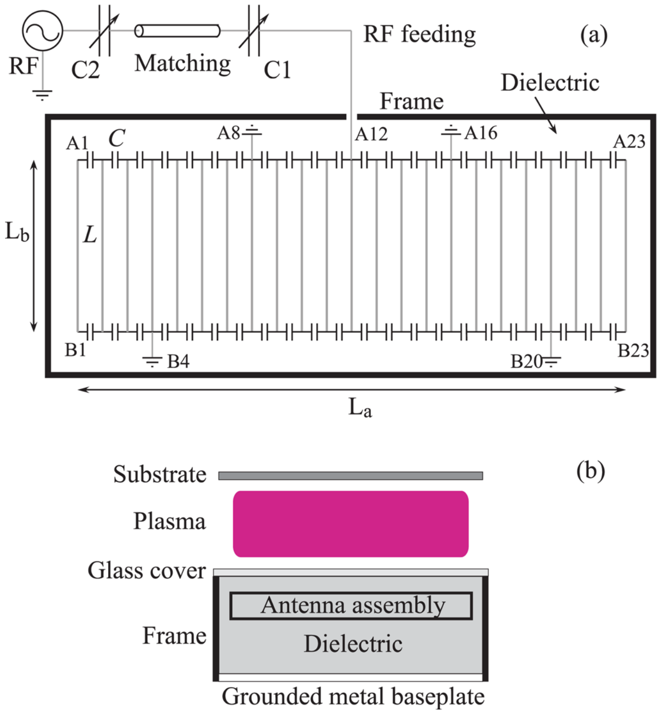

FIG. 3. (a) Schematic top view of the planar RF antenna showing the antenna bars (inductance L), the capacitors (C), and the matching network. (b) Schematic end view of the antenna showing the grounded metal baseplate, the metal frame sidewalls, and the antenna embedded in the dielectric with a protective glass cover. A substrate can be placed above the plasma as shown. The whole assembly is placed within the vacuum vessel.

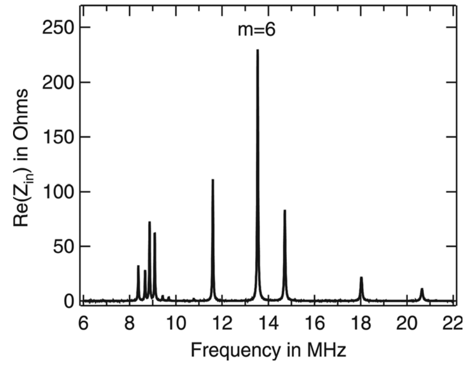

FIG. 4. Measured resonance spectrum of the 23-leg planar RF antenna. Figure taken from Ref. 8.

could be a limitation on the copper leg length (of the order of 1 m at this frequency) due to the wavelength of the standing wave.[11] Note also that the antenna is designed to operate at a fixed RF frequency of 13.56 MHz, which is allocated for industrial applications. The mode $m=6$ was chosen for a deeper study on the antenna performance, as it is easy to isolate, which generates higher RF currents in the legs than lower modes at comparable RF power and is better in terms of plasma uniformity. In order to match the frequency of this particular resonant mode with 13.56 MHz, high RF power capacitor assemblies with equivalent capacitance values of $C=2600$ pF are soldered to the copper legs by silver leads, whose inductance is measured to be $M=6$ nH. The inductance of each copper leg is 0.156μH. The antenna is fed by the RF power supply through the central leg $A12$ and connected to ground at four points $B4, A8, A16$, and $B20$ (see Fig. 3(a)). The copper tubes are water cooled to prevent excessive heating of the antenna components such as the capacitors. The principal heat load of the antenna is the plasma itself, not the ohmic heating of the antenna RF currents in the bars.

The RF power generator is connected to a specific matching network that has been developed on the basis of transmission line impedance transformation. It consists of a 1 m-long coaxial cable in series between two adjustable vacuum capacitors (C1 and C2 in Fig. 3(a)). The imaginary part of the input antenna impedance Z_{in} is brought to zero by tuning capacitor C2 alone, and the real part is brought to 50Ω by capacitor C1 and the transmission line.

The resonance spectrum of the antenna without plasma measured by a network analyzer is shown in Figure 4. The resonance frequency in vacuum is influenced by the mutual inductance between the bars, and by image currents induced in conducting screens, such as the baseplate and a metallic substrate. The real impedance value for each mode depends on the configuration connection. In our case of symmetric feeding and four connections to ground, the odd modes of resonance are forbidden by symmetry and the real part of the antenna impedance Z_{in} is maximal for the mode $m=6$ near 13.56 MHz. A high real input impedance value of the antenna implies that the RF input current I_{in} (see Fig. 3(a)) that flows from the RF generator into the antenna is minimal. This condition is crucial in order to keep the perturbations to the intrinsic resonant currents and voltages distributions (Eq. (2)) as small as possible. The resonance peaks visible at 14.70 MHz and 18.02 MHz have been identified as resonances of the system composed of the antenna and the four short connections to the grounded baseplate. They are not intrinsic modes of the antenna, and they can be shifted to other frequencies by changing the inductance of these connections.

Using a current transformer, a voltage probe, and a variable frequency RF generator, Fig. 5 shows the antenna impedance measured in detail around the mode $m=6$ with and without plasma. In both cases, the antenna behaves as a parallel resonant circuit, and the imaginary part of the impedances at the resonance frequencies is zero. The dominantly real input impedance near to antenna resonance avoids the problem of strong reactive currents and voltages in the matching box and RF power connections associated with conventional large-area plasma sources. The mutual inductance due to the plasma slightly increases the vacuum resonance frequency and strongly decreases the resonance Q-factor due to dissipation as shown in Fig. 5. It is observed that the real impedance value is typically divided by a factor of about 5 under high power plasma coupling. Furthermore, these impedance properties do not depend strongly on the size of the antenna, meaning that the RF matching is very convenient since the input impedance of the RF antenna is real and of the order of magnitude of 50Ω.

In order to further characterize the antenna experimentally, a B-dot probe is used to measure the distribution of currents in the legs. It can be seen in Figure 6(a) that the correspondence between the measurements and the calculated

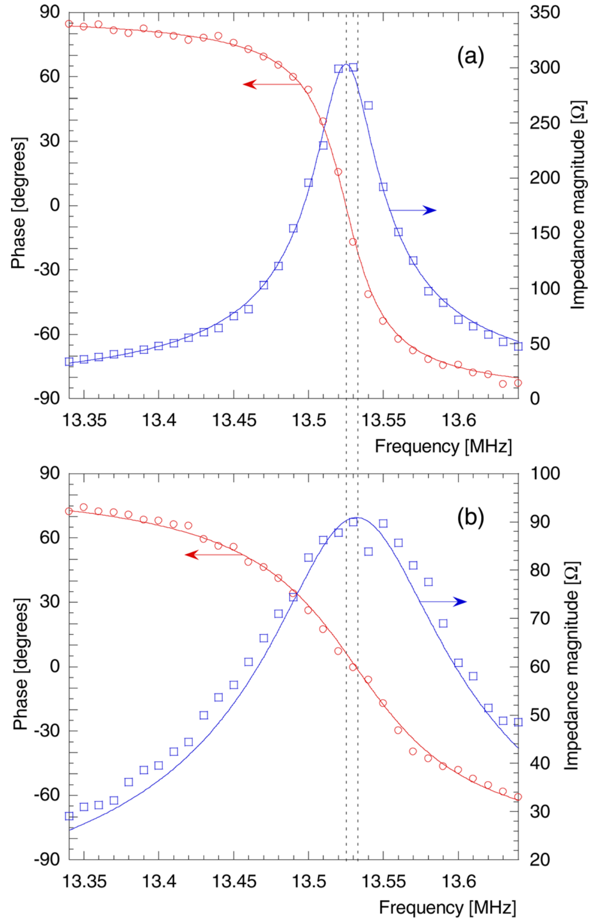

FIG. 5. The antenna impedance magnitude (squares) and phase (circles) measured in the neighborhood of the $m=6$ mode (a) without plasma; and (b) with a low power plasma (80 W). For comparison, the lines show fitted curves using a parallel resonance equivalent circuit for each case: (a) 13.13 nF in parallel with 10.55 nH and 2.65 m Ω in series; (b) 15.09 nF in parallel with 9.166 nH and 6.68 m Ω in series. The dotted lines show the shift in the resonance frequency from 13.525 MHz (in vacuum) to 13.532 MHz for the low power plasma.

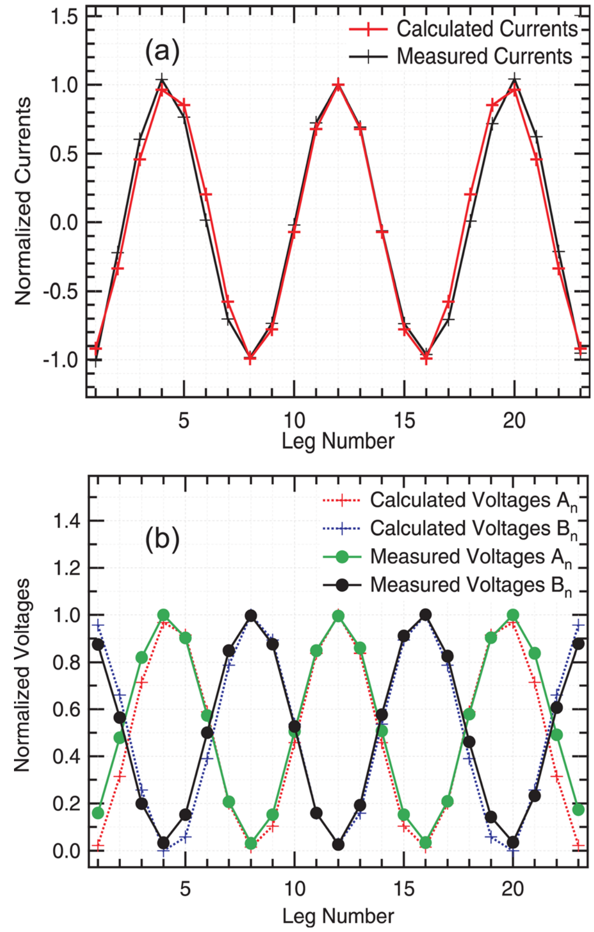

FIG. 6. (a) Calculated (red) and measured (black) current amplitudes in the legs of the planar RF antenna for the mode $m=6$. (b) Calculated (red and blue dashed-lines) and measured (green and black solid lines) voltage amplitudes at the nodes of the planar RF antenna for the mode $m=6$. Figure taken from Ref. 8.

distribution (Eqs. (2)–(4)) for the antenna excited in the mode $m=6$ is excellent. Small discrepancies are observed in the first and last third parts of the antenna; these slight differences are attributed to the mutual inductances between the legs that are not taken into account in the calculations. Similar effects are also visible in Figure 6(b) for the voltages at the A_n and B_n nodes. As expected from the calculations (Eqs. (2)–(4)), these current and voltage distributions are characterized by three wavelengths over the antenna length and are symmetric about the central leg.

A second measurement system containing 15 equally spaced single Langmuir probes arranged parallel to the antenna legs was built to measure the plasma density profile. The pins are made of steel wires 0.4 mm diameter and 4 mm long (the differences between the areas of the pins are estimated to be less than 10%). Moving this linear array of biased probes through the plasma along the antenna length gives the topography of the ion saturation current which is proportional to the electron density of the argon plasma. A small perturbation of the plasma is observed when moving the whole probe system.

IV. RESULTS

For an antenna operating in the mode $m=6$ at 13.56 MHz, argon plasmas have been ignited and sustained with RF power as low as 10 W and up to about 2000 W at pressures between 10^{-3} and 10^{-1} mbar. The physical behavior of the plasma corresponding to these conditions has been investigated in detail by varying the RF power.

Figure 7 shows an example of the electron density topography measured for an argon plasma at 1000 W along a plane in the middle of the 8 cm-gap between the antenna and a floating metallic substrate. Here, the electron density is maximal in the center and decreases rapidly near the sides. The electron density was measured by microwave interferometry to be above $10^{17}\mathrm{m}^{-3}$. Contour lines shown in Fig. 7 are plotted each 10% of electron density and show that it is symmetrical in both dimensions and presents a non-uniformity of less than $\pm 5\%$ in the central region (± 0.2 m along Ox and ± 0.08 m along Oy). Although the antenna is inductively coupled to the plasma, the image of the antenna current distribution is hardly visible in the plasma density. This is related to the low working gas pressure that favors diffusion of the plasma species into the entire plasma volume.

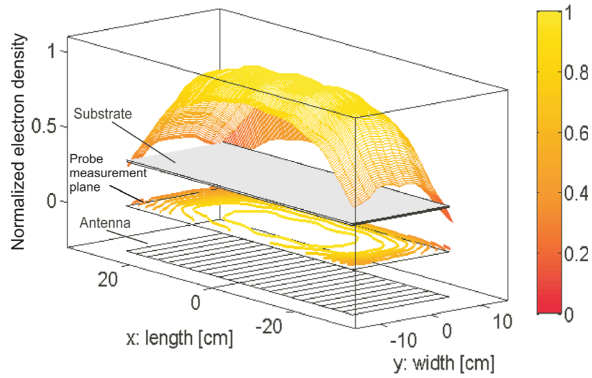

FIG. 7. Normalized electron density surface obtained with Langmuir probes at about 4 cm above the antenna and at a power of 1000 W. The Ar flux is 10 sccm and the pressure 10^{-2} mbar. A floating metallic substrate is placed 8 cm above the RF antenna. The level-lines in the contour plot are separated by 10%.

Figures 8(a) and 8(c) present two measured electron density patterns obtained at RF powers of 20 W and 1000 W, respectively, with the probe located only 2 cm above the antenna. The argon flux and pressure were kept constant at 50 sccm and $2 \cdot 10^{-2}$ mbar. The plasma profiles are not the same indicating that the plasma couples in two different ways with the antenna. These measurements are compared in Figs. 8(b) and 8(d) with two calculated electric field magnitude profiles at the same position using COMSOL MULTIPHYSICS program.[12]

In a first calculation (Fig. 8(b)), the physical parameters defining the RF antenna were its voltages at each node according to Eqs. (3). The electric field is then calculated in

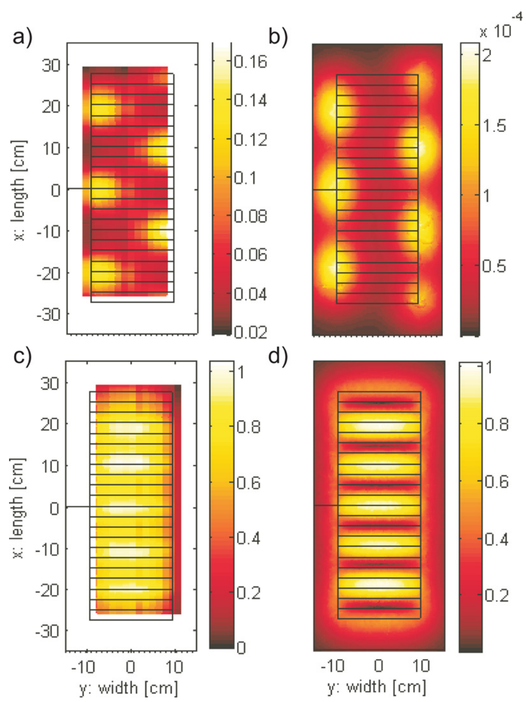

FIG. 8. Images (a) and (c) present measured electron density profiles at 20 W and 1000 W, respectively, at a distance of 2 cm from the antenna. The Ar flux is 50 sccm and the pressure is $2 \cdot 10^{-2}$ mbar. Images (b) and (d) present calculated electric field magnitude profiles in a parallel plane 2 cm above the antenna defined in the first case (b) by its voltages at each node and in the second case (d) by its voltages at each node and its currents in each segment.

a plane parallel to the antenna at the same distance from the antenna as the measurement, as follows:

$$|\vec{E}| = |-\overrightarrow{\nabla V}|. \tag{5}$$

In the second calculation (Fig. 8(d)), not only the voltages but also the different electric currents were taken into account in the calculation, using Ohm's law and the impedance of each segment of the antenna. Thereby an additional contribution to the electric field inside the plasma is added, due to electromagnetic induction.

$$|\vec{E}| = \left| -\overrightarrow{\nabla V} - \frac{\partial \vec{A}}{\partial t} \right|, \tag{6}$$

where $\vec{A}$ is the magnetic potential vector defined by $\vec{B} = \vec{\nabla} \times \vec{A}$. Comparison between the measurement and the simulation demonstrates that the plasma generated by the antenna at low power (Figs. 8(a) and 8(b)) is capacitively coupled with the antenna potentials. Both measured electron density and the calculated electric field magnitude show five areas of higher density located above the nodes where the RF voltages are maximal, that is to say nodes $A4, B8, A12, B16$ and $A20$ as shown in Figure 6(b). At higher RF power (Figs. 8(c) and 8(d)), a transition occurs into an inductive mode, in which the plasma couples with the RF currents in the antenna (see Figs. 6(a) and 9). The electron density is strongly increased in the areas above the legs carrying the maximum currents. The normalization of the scales for both "inductive" patterns (Figs. 8(c) and 8(d)) makes it clear that the electron density and the electric field are more than one order of magnitude larger than for the "capacitive" patterns (Figs. 8(a) and 8(b)).

The electron density profile in the inductive mode shown in Fig. 8(c) also shows elongated areas with maxima following the current distribution. The electron density along the middle of the antenna is given in Figure 9. These profiles broaden with increasing power from 100 W to 200 W and finally to 1000 W. Black marks indicate the position of the legs with maximal currents and correspond effectively to the local maxima of density. Notice how the two electron density maxima located near the edges of the antenna at ±20 cm

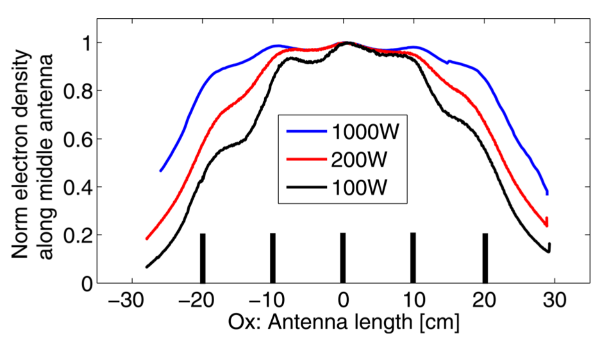

FIG. 9. Electron density profiles (normalized) along the RF antenna length at 100, 200, and 1000 W at a distance of 4 cm above the antenna. The Ar pressure is $7 \cdot 10^{-3}$ mbar, and the flux is 10 sccm. The black line segments indicate the positions of the legs with maximal currents, that is to say, leg number 4, 8, 12, 16, and 20, as in Fig. 6(a).

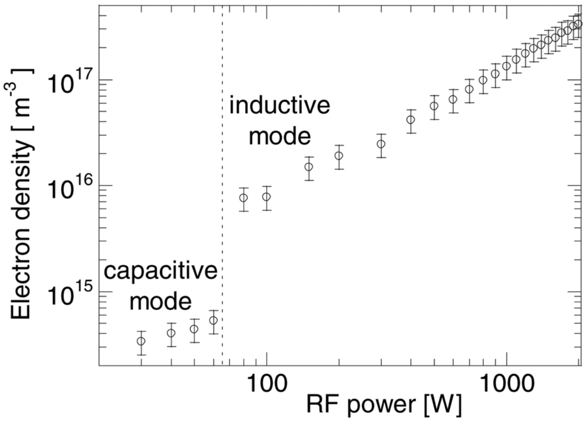

FIG. 10. Maximum electron density measured by 33 GHz interferometer in the Ar plasma for increasing RF power going from 30 W to 2000 W. The Ar pressure is 10^{-2} mbar, and the flux is 30 sccm. The transition from capacitive to inductive coupling occurs at around 60 W.

are progressively raised to the same values as the three maxima located near the central feeding, showing that the plasma becomes more and more uniform with increasing power. This indicates that the plasma ionization rate begins to dominate the diffusion loss process at the edges and extend the high electron density from the center of the antenna to the edges resulting in only ±5% non-uniformity over more than 75% of the antenna at 1000 W.

The aforementioned transition from the capacitive mode into the inductive mode has also been characterized by slowly increasing the RF power and measuring the average electron density along the antenna width using a 33 GHz microwave interferometer. Figure 10 shows the evolution of the electron density between 30 W and 2000 W; a clear step by more than one order of magnitude in electron density is observed around 60 W for an argon pressure of 10^{-2} mbar. In the inductive mode, the electron density increases monotonically with power and since no saturation was observed, even higher electron densities should be obtained above 2 kW.

V. CONCLUSION

A prototype of a HELYSSEN planar RF antenna operating at 13.56 MHz has been built and tested up to an RF power of 2000 W. The antenna itself constitutes a resonant structure for which the RF voltages and currents have been completely defined theoretically and measured experimentally with an excellent agreement.

Argon plasmas are easily ignited and couple capacitively with the antenna at low power (from 10 W to 60 W) and inductively above a threshold power of about 60 W. The plasma density profiles follow exactly the current distribution corresponding to the mode chosen for excitation, which in this case was the mode $m = 6$.

A plasma non-uniformity of less than ±5% in terms of electron density was measured at a few centimeters from the antenna. Electron densities above $10^{17} m^{-3}$ were measured by microwave interferometry at RF power above 1 kW.

These promising results encourage further development to increase the area of the antenna as well as the excitation power in order to improve the performance of this type of RF plasma source. In parallel, PECVD process tests using this RF antenna will be undertaken in collaboration with industry.

ACKNOWLEDGMENTS

The authors thank Frédéric Moix for his contribution to the experiments during his Master thesis. This work was supported by the Swiss Commission for Technology and Innovation (CTI) under Research Grant No. 9896.2 PFIW-IW.

[1]M. A. Lieberman and A. J. Lichtenberg, *Principles of Plasma Discharges and Materials Processing* (Wiley-Interscience, 2005).
[2]H. Chatham, Surf. Coat. Technol. **78**, 1 (1996).
[3]F. F. Chen, *Lecture Notes on Principles of Plasma Processing* (Kluwer, 2003).
[4]J. Perrin, J. Schmitt, C. Hollenstein, A. Howling, and L. Sansonnens, Plasma Phys. Controlled Fusion **42**, B353 (2000).
[5]J. Hopwood, Plasma Sources Sci. Technol. **1**, 109 (1992).
[6]A. E. Wendt and L. J. Mahoney, Pure Appl. Chem. **68**, 1055 (1996).
[7]P. Guittienne, see http://www.sumobrain.com/patents/WO2010092433.html for Apparatus for large area plasma processing (August 2010).
[8]S. Lecoultre, Ph. Guittienne, A. A. Howling, P. Fayet, and Ch. Hollenstein, J. Phys. D: Appl. Phys. **45**, 082001 (2012).
[9]J. Jin, *Electromagnetic Analysis and Designs in Magnetic Resonance Imaging* (CRC, 1998).
[10]P. Guittienne and E. Chevalier, J. Appl. Phys. **98**, 083304 (2005).
[11]M. A. Lieberman, J. P. Booth, P. Chabert, J. M. Rax, and M. M. Turner, Plasma Sources Sci. Technol. **11**, 283 (2002).
[12]See http://www.comsol.com for information about the finite-element solver.